Acta Mechanica 141, 201 – 223 (2000)

ACTA MECHANICA

Numerical investigation of two-dimensional turbulent boundary-layer compressible flow with adverse pressure gradient and heat and mass transfer

N. G. Kafoussias and **M. A. Xenos,** Patras, Greece

(Received January 26, 1999)

Summary. The effect of heat and mass transfer on the steady turbulent compressible boundary-layer flow with adverse pressure gradient are numerically studied. The Reynolds-averaged boundary-layer equations and their boundary conditions are transformed, in a suitable form for numerical solution, by using the compressible version of the Falkner-Skan transformation and the resulting coupled and nonlinear system of partial differential equations is solved using the Keller's-box method and a modified version of it. For the eddy kinematic viscosity the model developed by Cebeci and Smith is employed whereas for the turbulent Prandtl number model a modification of the extended Kays and Crawford's model is used. Numerical calculations are carried out for the case of air, at about free stream temperature of 300 °K, and for a linearly retarded flow, known as Howarth's flow when the porous limiting surface is adiabatic, heated or cooled. The porous surface is subjected to a continuous or localized suction/injection velocity and the influence of this velocity as well as of the free-stream Mach number and of the heat-transfer parameter on the turbulent boundary-layer and the separation point is examined. It is hoped that in the absence of detailed investigations into this problem, the obtained results, presented in the figures, are very interesting and give a clearer insight into the mechanism of controlling a turbulent boundary-layer compressible flow.

1 Introduction

It is known that most flows, which occur in practical applications, are turbulent, the term denoting a motion in which an irregular fluctuation is superimposed on the main stream. This irregular fluctuation (mixing, or eddying motion) is responsible for the large resistance experienced by turbulent flow in pipes, for the drag encountered by ships and aeroplanes and for the losses in turbines and turbocompressors. The simplest case of a turbulent boundary-layer occurs on a flat plate at zero incidence. This flow model is, however, of great practical importance and it can be used in the calculation of the skin-friction drag on ships, on lifting surfaces and aeroplane bodies in aeronautical engineering, and on the blades of turbines and rotary compressors [1].

Apart from skin-friction drag we are interested in knowing whether the turbulent boundary-layer will separate under given circumstances and if so, it would be useful to determine the point of separation. Separation is mostly an undesirable phenomenon because it entails large energy losses and for this reason methods have been devised for the artificial prevention of it. As widely known, control of flow separation is generally associated for engineering

applications with an increase in performance, because of the detrimental effect of separation on drag and pressure recovery [2], [3]. For a two-dimensional steady flow, separation can be prevented or delayed by applying basic active and passive control approaches such as suction, blowing, passive devices, surface cooling, etc. Such control techniques have been currently employed via vortex generators on the wings of some Boeing aircraft, via blown flaps on older generation supersonic fighters or leading edge extensions and strakes on newer generations [4]. In two-dimensional flows on the upper side of a wing, vortex generators are set and designed to produce a gentle streamwise vortex that re-energizes the mean wall flow in the near-wall region, to overcome the adverse pressure gradient.

The various hypotheses which have been advanced to explain how flow control devices act on turbulent boundary-layer and flow separation depend upon considerations of the turbulent boundary-layer itself and a complete description of turbulent boundary-layer structure can be found in [5]–[8]. Although there is still no accepted theory, which really details the structural behavior of turbulent flows, yet, the most acceptable technique for turbulent boundary-layer control is the suction/injection technique. Suction has been very often used as an aerodynamic flow control technique to prevent laminar to turbulent boundary-layer transition as well as turbulent flow separation. Recent experiments with application of suction along the leading edge of a wing revealed the possibility, under appropriate conditions, to delay leading edge contamination [9]. For turbulent boundary layers, suction has been applied onto aerofoils in order to prevent separation. The needed suction rate coefficient C_q, defined as the ratio of the suction velocity $|v_0|$ to the free stream velocity $u_\infty (C_q = |v_0|/u_\infty)$, was relatively low, typically in the range of 0.002 to 0.004 [10]. Optimally, for high lift configurations, suction should be concentrated on the low pressure side of the aerofoil, just a short distance downstream of the nose where, at high values of the angle of attack, large adverse pressure gradient was occur [2].

On the other hand, Sokolov and Antonia [11] studied the response of a turbulent boundary-layer to *intense wall suction* through a 40 mm porous strip, at low momentum thickness Reynolds number. An extensive number of studies, involving either large discrete holes or small uniformly distributed holes, have been used to apply suction through a surface for turbulent boundary-layer control. Available literature indicates that porous surfaces are capable of providing nearly uniform suction, with smaller drag increases at a given suction rate, than the more abrupt, discrete holes or slots. Wilkinson et al. [12] developed what is called *an hybrid suction surface* for turbulent flows. It is a slotted suction surface which consists of an array of closely spaced slots aligned in the direction of the mean streamwise flow. Gad-el-Hak and Blackwelder [13] suggested an approach which is called *selective suction*, in which small amounts of suction were applied below the low-speed streaks in order to reduce the intensity of the ejections of low-speed streaks outwards from the wall and to slow or disrupt the bursting process. Selective suction has also been very recently considered for controlling streamwise vortices, generated by Görtler instability developing on a concave wall and it was found that rather low values of suction flow rate were sufficient for delaying significantly the breakdown of vortices [14].

Another possibility for turbulent boundary-layer control is to use a *localized suction* that is to apply continuous suction in a region confined between $x = a$, and $x = b, 0 < a < b \ll L$, where L is the whole length of the boundary surface. Fundamental wind tunnel experiments performed by Reynolds and Saric [15] indicated that suction is more effective when applied at Reynolds number close to the lower branch of the neutral curve, in qualitative agreement with previous theoretical results [16]. Finally, another way of turbulent boundary-layer control is by *heating or cooling the wall* or by blowing air from slots, multiple slots or holes. By

blowing air the skin friction in case of turbulent boundary-layers can be reduced. As regards skin friction reduction by blowing, several parameters are of prime importance, such as the injection rate coefficient, the injection angle, the slot-lip thickness and so forth. Slot efficiency is rather well detailed in [17] whereas tangential blowing has been shown to be a correct candidate for improving control of aircraft flying at high angles of attack [18]. Furthermore, a Direct Numerical Simulation (DNS) of a fully developed turbulent channel flow with uniform injection has been also considered by Sumitani and Kasagi [19]. It has been found that injection has an inverse influence compared to uniform suction, that is, it decreases the friction coefficient and strengthens the near wall turbulence activity.

As already mentioned before, the problem of turbulent boundary-layer control is a broad one and a great deal of research has been recently done on this subject, numerically or experimentally [20]–[23]. However, there has been much less work on documentation of adverse pressure gradient effects, on the separation of the compressible turbulent boundary-layer, in the presence of heat and mass transfer. This is one of the most important problems in aerodynamics because for a reliable study of the compressible turbulent boundary-layer it is necessary and important to quantify its sensitivity to various control parameters such as Mach number, pressure gradient, heat transfer parameter and wall mass transfer parameter.

Therefore, in this work an attempt is undertaken for the numerical investigation of the two-dimensional turbulent boundary-layer compressible flow, over a finite smooth and permeable flat surface, with an adverse pressure gradient and heat and mass transfer. The mathematical formulation of the problem is presented in Sect. 2, whereas in Sect. 3 the adopted eddy-viscosity and turbulent-Prandtl number formulation is presented. In Sect. 4 the numerical solution of the problem is obtained by using the Keller's-box method, or a modified version of it, for the case of a linearly retarded flow, and for the case of continuous suction/injection applied on the porous surface for three different cases of the dimensionless heat-transfer parameter S_w. The case of localized suction/injection is also examined. Finally, in Sect. 5, a detailed analysis of the obtained results is presented, for different values of the dimensionless parameters entering into the problem under consideration, followed by the concluding remarks presented in Sect. 6.

2 Formulation of the problem and mathematical analysis

We consider the steady two-dimensional compressible turbulent boundary-layer flow over a smooth flat permeable surface. The surface is located at

$$y = 0\,, \qquad 0 \leq x \leq L\,, \qquad -\infty < z < +\infty$$

and is parallel to the free-stream of a heat-conducting perfect gas flowing with velocity u_∞. The equations governing this type of flow are the Reynolds-averaged boundary-layer equations which can be written, in orthogonal coordinates (x, y), as follows:

continuity equation

$$\frac{\partial}{\partial x}\left(\overline{\varrho}\,\overline{u} + \overline{\varrho' u'}\right) + \frac{\partial}{\partial y}\left(\overline{\varrho}\,\overline{v} + \overline{\varrho' v'}\right) = 0\,; \tag{1}$$

x-momentum equation

$$\left(\overline{\varrho}\,\overline{u} + \overline{\varrho' u'}\right)\frac{\partial \overline{u}}{\partial x} + \left(\overline{\varrho}\,\overline{v} + \overline{\varrho' v'}\right)\frac{\partial \overline{u}}{\partial y} = -\frac{\partial \overline{p}}{\partial x} + \frac{\partial}{\partial y}\left[\mu\frac{\partial \overline{u}}{\partial y} - \left(\overline{\varrho u' v'} + \overline{\varrho' u' v'}\right)\right]; \tag{2}$$

y-momentum equation

$$\frac{\partial \overline{p}}{\partial y} = 0\,; \tag{3}$$

total-enthalphy equation

$$\overline{\varrho}\,\overline{u}\,\frac{\partial H}{\partial x} + (\overline{\varrho}\,\overline{v} + \overline{\varrho' v'})\,\frac{\partial H}{\partial y} = \frac{\partial}{\partial y}\left[k\,\frac{\partial \overline{T}}{\partial y} - c_p\overline{\varrho}\,\overline{T'v'} - c_p\overline{\varrho' T' v'} + \overline{u}\left(\mu\,\frac{\partial \overline{u}}{\partial y} - \overline{\varrho}\,\overline{u'v'} - \overline{\varrho' u' v'}\right)\right]. \tag{4}$$

In the above equations the symbols presented have their usual meaning in aerodynamics and we also have replaced the instantaneous "quantities" f (e.g. u, v, T, ϱ) by the sum of their mean ($\overline{f}$) and fluctuating parts (f'), that is $f = \overline{f} + f'$.

It can be proved, by applying an order-of-magnitude analysis [24], that density fluctuations are generally small in practice, both in low-speed flows with high heat transfer and in high-speed adiabatic-wall flows. Thus, terms containing ϱ' can be dropped from the mass, momentum and enthalpy equations for thin shear layers. Also, the term $\overline{\varrho' u'}$ is negligible compared with $\overline{\varrho}\,\overline{u}$ as long as $(\gamma - 1)M^2$ is not an order of magnitude greater than unity, whereas the term $\overline{\varrho' v'}$ cannot be neglected, compared with $\overline{\varrho}\,\overline{v}$, in the continuity, momentum and total-enthalpy equations.

On the other hand, the y-momentum equation (3) shows that the pressure variation is governed by the free-stream and, with the use of Bernoulli's equation, the term $\partial \overline{p}/\partial x$ in the x-momentum equation can be substituted by

$$-\frac{\partial \overline{p}}{\partial x} = -\frac{d\overline{p}}{dx} = \varrho_e u_e \frac{du_e}{dx}\,, \tag{5}$$

where the subscript e refers to the conditions at the edge of the boundary-layer.
Using the abbreviation $\overline{\varrho v}$ for $\overline{\varrho}\,\overline{v} + \overline{\varrho' v'}$ and omitting, for simplicity, the overbars on the basic time-average variables u, v, p, ϱ and T the equations of the problem can be written now as

$$\frac{\partial}{\partial x}(\varrho u) + \frac{\partial}{\partial y}(\overline{\varrho v}) = 0\,, \tag{6}$$

$$\varrho u\,\frac{\partial u}{\partial x} + \overline{\varrho v}\,\frac{\partial u}{\partial y} = \varrho_e u_e \frac{du_e}{dx} + \frac{\partial}{\partial y}\left[\mu \frac{\partial u}{\partial y} - \varrho\overline{u'v'}\right], \tag{7}$$

$$\varrho u\,\frac{\partial H}{\partial x} + \overline{\varrho v}\,\frac{\partial H}{\partial y} = \frac{\partial}{\partial y}\left[k\,\frac{\partial T}{\partial y} - c_p\varrho\overline{T'v'} + u\left(\mu\,\frac{\partial u}{\partial y} - \varrho\overline{u'v'}\right)\right]. \tag{8}$$

The parabolic nature of the above equations requires that boundary conditions must be provided on two sides of the solution domain in addition to the initial conditions at $x = x_0$. So, the boundary conditions of the problem under consideration are

$$\begin{aligned} &y = 0: \qquad u = 0\,, \qquad v = v_w(x)\,, \qquad H = H_w(x)\,, \\ &y = \delta: \qquad u = u_e(x)\,, \qquad H = H_e(x)\,, \end{aligned} \tag{9}$$

where δ is a distance sufficiently far away from the wall where the u velocity and total enthalpy H reach their free-stream values and $v_w(x)$ is the mass transfer velocity at the wall. In the case of an impermeable wall $v_w(x)$ is equal to zero. It is worth mentioning here that the

total enthalpy H for a perfect gas is defined by the expression

$$H = c_p T + \frac{1}{2} u^2 \tag{10}$$

and consequently the boundary conditions (9), referring to the total enthalpy H on the wall and free-stream, become

$$y = 0: \quad T = T_w(x), \qquad y = \delta: \quad H = H_e(x) = c_p T_e(x) + \frac{1}{2} u_e{}^2(x). \tag{11}$$

Before Eqs. (6)–(8) can be solved for a turbulent flow, subjected to the boundary conditions (9), it is necessary to incorporate a model for the Reynolds stress terms $-\varrho\overline{u'v'}$ and $-c_p\varrho\overline{T'v'}$.

For the shear stress $-\varrho\overline{u'v'}$, in a two-dimensional thin shear layer, the eddy kinematic viscosity ε_m can be defined by the expression

$$\varepsilon_m = \frac{-\overline{u'v'}}{\dfrac{\partial u}{\partial y}}, \tag{12}$$

whereas the eddy diffusivity of heat, for the turbulent heat flux rate, can be defined by

$$\varepsilon_h = \frac{-\overline{T'v'}}{\dfrac{\partial T}{\partial y}}. \tag{13}$$

The ratio $\varepsilon_m/\varepsilon_h$, of the above quantities, is called turbulent Prandtl number Pr_t by analogy with the molecular Prandtl number $\mathrm{Pr} = \mu c_p/k$.

So, with eddy kinematic viscosity ε_m and turbulent Prandtl number Pr_t, defined by the expressions

$$-\overline{u'v'} = \varepsilon_m \frac{\partial u}{\partial y}, \qquad -\overline{T'v'} = \frac{\varepsilon_m}{\mathrm{Pr}_t} \frac{\partial T}{\partial y}, \tag{14}$$

the equations describing the problem under consideration can be written as

$$\frac{\partial}{\partial x}(\varrho u) + \frac{\partial}{\partial y}(\overline{\varrho v}) = 0, \tag{15}$$

$$\varrho u \frac{\partial u}{\partial x} + \overline{\varrho v} \frac{\partial u}{\partial y} = \varrho_e u_e \frac{du_e}{dx} + \frac{\partial}{\partial y}\left[(\mu + \varrho\varepsilon_m)\frac{\partial u}{\partial y}\right], \tag{16}$$

$$\varrho u \frac{\partial H}{\partial x} + \overline{\varrho v} \frac{\partial H}{\partial y} = \frac{\partial}{\partial y}\left\{\left(\frac{\mu}{\mathrm{Pr}} + \varrho \frac{\varepsilon_m}{\mathrm{Pr}_t}\right)\frac{\partial H}{\partial y} + \left[\mu\left(1 - \frac{1}{\mathrm{Pr}}\right) + \varrho\varepsilon_m\left(1 - \frac{1}{\mathrm{Pr}_t}\right)\right] u \frac{\partial u}{\partial y}\right\}, \tag{17}$$

$$\begin{aligned} &y = 0: \quad u = 0, \quad v = v_w(x), \quad H = H_w(x), \\ &y = \delta: \quad u = u_e(x), \quad H = H_e(x). \end{aligned} \tag{18}$$

It is useful to express the governing equations (15)–(17), subjected to the boundary conditions (18), in transformed variables before they are solved. For this purpose we introduce the compressible version of the Falkner-Skan transformation, defined by

$$\eta(x, y) = \int_0^y \sqrt{\frac{u_e(x)}{\nu_e(x)x}} \frac{\varrho(x, y)}{\varrho_e(x)}\, dy, \tag{19}$$

$$\psi(x, y) = \sqrt{\varrho_e \mu_e u_e x}\, f(x, \eta) \tag{20}$$

and the definition of the stream function ψ, for a compressible flow, that satisfies the continuity equation (15), by the relations

$$\varrho u = \frac{\partial \psi}{\partial y}, \qquad \overline{\varrho v} = -\frac{\partial \psi}{\partial x}. \tag{21}$$

On introducing also the dimensionless total-enthalpy ratio $S(x,\eta) = H/H_e$, besides the dimensionless velocity $f' = u/u_e$, the system of Eqs. (16)–(18) become

$$(bf'')' + m_1 f f'' + m_2[c - (f')^2] = x\left\{f'\frac{\partial f'}{\partial x} - f''\frac{\partial f}{\partial x}\right\}, \tag{22}$$

$$(eS' + df'f'')' + m_1 f S' = x\left\{f'\frac{\partial S}{\partial x} - S'\frac{\partial f}{\partial x}\right\}, \tag{23}$$

$$\begin{aligned} &\eta = 0: \quad f' = 0, \quad f_w(x) = f(x,0) = -\frac{1}{(u_e\mu_e\varrho_e x)^{1/2}}\int_0^x \varrho_w(x,0)v_w(x)\,dx, \quad S = S_w(x,0), \\ &\eta = \eta_e: \quad f' = 1, \quad S = 1, \end{aligned} \tag{24}$$

where primes denote partial differentiation with respect to η $\left(()' = \partial()/\partial\eta\right)$ and the quantities b, m_1, m_2, etc. are defined as follows

$$\begin{aligned} &b = C(1+\varepsilon_m^+), \qquad C = \frac{\varrho(x,\eta)\,\mu(x,\eta)}{\varrho_e(x)\,\mu_e(x)}, \qquad c = \frac{\varrho_e(x)}{\varrho(x,\eta)}, \\ &d = \frac{Cu_e{}^2(x)}{H_e(x)}\left[1 - \frac{1}{\mathrm{Pr}} + \varepsilon_m^+\left(1 - \frac{1}{\mathrm{Pr}_t}\right)\right], \qquad \varepsilon_m^+ = \frac{\varepsilon_m}{\nu(x,\eta)}, \\ &e = \frac{C}{\mathrm{Pr}}\left(1 + \varepsilon_m^+\frac{\mathrm{Pr}}{\mathrm{Pr}_t}\right), \qquad m_2 = \frac{x}{u_e(x)}\frac{du_e(x)}{dx}, \qquad R_x = \frac{u_e(x)\,x}{\nu_e(x)} \quad \text{and} \\ &m_1 = \frac{1}{2}\left[1 + m_2 + \frac{x}{\varrho_e(x)\,\mu_e(x)}\frac{d}{dx}(\varrho_e\mu_e)\right]. \end{aligned} \tag{25}$$

It is worth emphasizing here that in the case of compressible laminar flow, the eddy kinematic viscosity ε_m and the turbulent Prandtl number Pr_t are zero and the quantities b, d and e are then defined as

$$b = C, \qquad d = \frac{Cu_e{}^2(x)}{H_e(x)}\left(1 - \frac{1}{\mathrm{Pr}}\right) \quad \text{and} \quad e = \frac{b}{\mathrm{Pr}}. \tag{26}$$

So, the compressible turbulent boundary-layer flow, with heat and mass transfer, is finally governed by the system of Eqs. (22)–(25). In this case, as in many cases, the turbulent boundary-layer flow equations remain parabolic and can be solved in the same manner as the laminar-flow equations. However, before proceeding to the numerical solution of this system of equations we have to adopt a turbulence model.

3 The turbulence model

There are several eddy-viscosity and turbulent-Prandtl-number formulations that can be used to represent ε_m^+ and Pr_t. For the eddy kinematic viscosity ε_m we employ the one developed by Cebeci and Smith [25] which is described in detail in [24]. This model is one of the simplest

with acceptable generality and it's accuracy has been explored for a wide range of flows for which there are experimental data. It has also been found that it gives results sufficiently accurate for most engineering problems [24], [26]. According to this formulation, the turbulent boundary layer in external and nonmerging internal flows is treated as a composite layer consisting of inner and outer regions with separate expressions for the eddy viscosity in each. On the other hand, different expressions have been proposed for the turbulent Prandtl number Pr_t. Cebeci [27] adopted van Driest's idea of near-wall damping of the mixing length to propose a turbulent Prandtl number concept. This model was extended by Chen and Chiou [28] for liquid metal flow in pipes in incorporating the enthalpy thickness δ_T in turbulent Prandtl number Pr_t. Jischa and Rieke [29] developed a model for Pr_t from the modeled transport equations given by the expression

$$\mathrm{Pr}_t = 0.9 + \frac{182.4}{\mathrm{Pr}\,\mathrm{R}_x^{0.888}} \,. \tag{27}$$

Kays and Crawford [30] developed a prediction model for Pr_t which can be used for all molecular Prandtl numbers and which is given by

$$\mathrm{Pr}_t = 1 \Big/ \left\{ \frac{1}{2\mathrm{Pr}_{t\infty}} + C\,\mathrm{Pe}_t \sqrt{\frac{1}{\mathrm{Pr}_{t\infty}}} - (C\,\mathrm{Pe}_t)^2 \left[1 - \exp\left(- \frac{1}{C\,\mathrm{Pe}_t \sqrt{\mathrm{Pr}_{t\infty}}} \right) \right] \right\} , \tag{28}$$

where

$$\mathrm{Pe}_t = \mathrm{Pr}\,\varepsilon_m^+ , \tag{29}$$

$\mathrm{Pr}_{t\infty}$ is the value of Pr_t far away from the wall and $C = 0.3$ is a constant prescribing the spatial distribution of Pr_t versus Pe_t.

In the model originally proposed by Kays and Crawford [30], $\mathrm{Pr}_{t\infty}$ was fixed to a constant value of 0.85. This has the disadvantage that Pr_t is always smaller than 1.7 and introduces an undesired behavior into the model, because for $\mathrm{Pr} \to 0$ heat will be transferred exclusively by molecular conduction and, therefore, Pr_t should tend to a large value.

On the other hand, the model for Pr_t, which is given by Eq. (27), does not consider the spatial distribution of Pr_t and, therefore, the value for Pr_t given by Eq. (27) can be seen as a mean value of Pr_t across the whole boundary layer. In order to overcome the above-mentioned undesired behaviors of models in [29] and [30], Weigand et al. [31] adopted a combination of both models in which they use the functional form of Pr_t developed by Jischa and Rieke [29] as an approximation for $\mathrm{Pr}_{t\infty}$ in Eq. (28). This model for Pr_t is also adopted in the present analysis ([31]). Moreover, for the approximation of the turbulent Prandtl number $\mathrm{Pr}_{t\infty}$, far away of the limiting surface (wall), we used the expressions

$$\mathrm{Pr}_{t\infty} = 0.9 + \frac{182.4}{\mathrm{Pr}\,\mathrm{R}_{\infty,x}^{0.888}} \,, \tag{30}$$

where

$$\mathrm{R}_{\infty,x} = \frac{u_\infty x}{\nu_\infty} \,. \tag{31}$$

4 Numerical solution of the problem

The aim of this work is the study of the two-dimensional compressible turbulent boundary-layer flow with adverse pressure gradient and heat and mass transfer. To show the effect of heat and mass transfer on the compressible turbulent boundary-layer flow over a porous sur-

face, in the presence of an adverse pressure gradient we consider, as an example, the linearly retarded flow, known as Howarth's flow. In this flow model the external velocity varies linearly with x, that is

$$u_e(\bar{x}) = u_\infty(1 - \bar{x}), \tag{32}$$

where u_∞ is the free-stream velocity, $\bar{x} = x/L$ and L is the length of the boundary permeable surface (porous wall). This flow model can be interpreted, for instance, as representing the potential flow along a flat wall which starts at $\bar{x} = 0$ and which abuts on to another infinite wall at right angles to it at $\bar{x} = 1 (x = L)$ [1]. For the numerical calculations the length L was taken equal to 8 m so that x varies between $x = 0$ and $x = 8$ m.
In such a case and according to its definition, Eq. (25), the dimensionless pressure gradient parameter m_2 is given by the expression

$$m_2 = m_2(x) = -\frac{\bar{x}}{(1 - \bar{x})} = -\frac{x}{(8 - x)}. \tag{33}$$

In most practical boundary-layer calculations, involving pressure gradient, it is necessary to predict the boundary-layer over its whole length. That is, for a given external velocity distribution and wall-temperature or heat-flux distribution and for a given transition point, it is necessary to calculate the laminar, transitional and turbulent boundary-layers, starting the calculations at the leading edge ($x = 0$). Starting from the leading edge, there is first a region ($0 < \mathrm{R}_x < \mathrm{R}_{xtr}$) in which the flow is laminar. After a certain distance, there is a region ($\mathrm{R}_{xtr} < \mathrm{R}_x < \mathrm{R}_{xt}$) in which the flow is transitional and in the third and last region ($\mathrm{R}_x \geq \mathrm{R}_{xt}$) the flow is fully turbulent.

It is known that the transitional Reynolds number R_{xtr}, at the start of transition, depends partly upon the turbulence in the free stream and greatly upon the surface conditions such as heating or cooling and smoothness or roughness. This number may be as low as 4×10^5 or as high as 4×10^6 [24]. For instance, if the plate is heated, the location of natural transition in a gas flow moves upstream, decreasing the value of the transitional Reynolds number, whereas if the plate is cooled, the location of transition moves downstream.

In this work we assume that the fluid is air (perfect gas), at about $T_\infty = 300\,^\circ\mathrm{K}$ ($\mathrm{Pr} = 0.708$) and we consider three different cases for the dimensionless total-enthalpy ratio on the wall (heat-transfer parameter $S_w = H_w/H_e$), thus covering the cases in which the wall is heated ($S_w = 2$), adiabatic ($S_w = 1$) and cooled ($S_w = 0.5$), respectively. It is worth mentioning here that the dimensionless heat-transfer parameter $S_w \neq 1$ corresponds to a flow with heat transfer, whereas the requirement $S_w = 1$ corresponds to a flow with no heat transfer between the wall and the fluid (adiabatic flow). On the other hand, the value $S_w = 2\,(S_w > 1)$ corresponds to the case of heating of the wall whereas the value $S_w = 0.5\,(S_w < 1)$ to the case of cooling of the wall.

So, in our study the calculations were started as laminar at $x = 0$ and transition was specified at (i) $x_{tr} = 0.066$ m for the case $S_w = 1\,(\mathrm{R}_{xtr} = 22 \times 10^5)$, (ii) $x_{tr} = 0.012$ for the case $S_w = 2\,(\mathrm{R}_{xtr} = 4 \times 10^5)$ and (iii) $x_{tr} = 0.12$ for the case $S_w = 0.5\,(\mathrm{R}_{xtr} = 4 \times 10^6)$ assuming that after these points the flow is fully turbulent. However, we could also assume that the flow was turbulent from the leading edge ($x_{tr} = 0$).

For the numerical study of the problem under consideration we have to solve the system of Eqs. (22) and (23) subjected to the boundary conditions (24). This system of equations is of parabolic type and it can be solved by using several numerical methods discussed in Cebeci and Smith [25], Cebeci and Bradshaw [24], Schreier [32], and in Minkowycz et al. [26]. The numerical scheme used to solve the system of Eqs. (22)–(24) is the well-known Keller's-box

numerical scheme [33], described in detail in [25] and [24], and a modified version of this scheme described in [34] and [35].

One of the requirements of the Keller's-box method is that the governing equations are written as first-order system and derivatives of $f(x,\eta), S(x,\eta)$ with respect to η are introduced as new functions. The resulting first-order system of equations is solved on an nonuniform rectangular net with centered-difference derivatives and averages at the midpoints of the net rectangle to get finite-difference equations with a truncation error of order $(\Delta\eta)^2 + (\Delta x^2)$. The resulting difference equations are implicit and nonlinear and they are linearized and solved by a block-elimination method. However, it was found that the usual central difference approximation in the x direction give rise to large but bounded oscillations in the numerical solutions, especially for large values of the suction/injection velocity $v_w(x)$, imposed at the wall. The oscillations reduce in magnitude as the x step is reduced, but their entire elimination requires an extremely small streamwise steplength. Therefore, it was decided, in such a case, to use a backward difference modification to the Keller's-box method and the solutions obtained, though now formally only first-order accurate in x, showed no sign of oscillations even for large step lengths. The resulting nonlinear algebraic system is solved using a multi-dimensional Newton-Raphson iteration scheme where the Jacobian (or iteration) matrix is computed numerically rather than being prescribed by the programmer. This technique has been used successfully in other recent papers where the explicit specification of the Jacobian is extremely lengthy [34], [35].

As it was stated earlier numerical calculations were carried out for air, at about $T_\infty = 300\,^\circ\mathrm{K}$ ($\mathrm{Pr} = 0.708$), for $S_w = H_w/H_e = 2, 1$ and 0.5, thus covering the cases in which the wall is heated, adiabatic and cooled, respectively.

The free-stream values $\mu_\infty, u_\infty, \varrho_\infty$ and H_∞ were calculated from the formulae

$$\mu_\infty = 1.45 \times 10^{-6} T_\infty^{3/2}/(T_\infty + 110.33) \quad \text{(Sutherland's law)}, \tag{34}$$

$$u_\infty = 20.04\, M_\infty \sqrt{T_\infty}, \tag{35}$$

$$\varrho_\infty = \frac{P_\infty}{287 T_\infty}, \tag{36}$$

$$H_\infty = 1005.7 T_\infty + \frac{1}{2} u_\infty^2 \qquad (c_p = 1005.7) \tag{37}$$

for different values of the free-stream Mach number M_∞, whereas the edge values T_e and P_e where calculated by using the formulae

$$T_e = T_\infty \left\{ 1 - \frac{\gamma - 1}{2} \mathrm{M}_\infty^2 \left[\left(\frac{u_e}{u_\infty} \right)^2 - 1 \right] \right\}, \qquad P_e = P_\infty \left(\frac{T_e}{T_\infty} \right)^{\gamma/(\gamma-1)}, \tag{38}$$

where $\gamma = c_p/c_v = 1.4$.

The edge values μ_e, ϱ_e and H_e were calculated by using formulas identical to those given by Eqs. (34), (36) and (37), respectively, except that free stream values (∞) of temperature, pressure and velocity were replaced by their edge values (e). It is worth mentioning here that Sutherland's law, Eq. (34), is an adequate approximation for the variation of viscosity μ with temperature T, for air. For viscous fluids, Ling and Dybbs [36] suggested a viscosity dependence on temperature T of the form:

$$\mu = \frac{\mu_\infty}{[1 + \gamma^*(T - T_\infty)]}, \tag{39}$$

so that viscosity is an inverse linear function of temperature T. Eq. (39) can also be written as

$$\frac{1}{\mu} = \alpha(T - T_r)\,, \tag{40}$$

$$\text{where} \quad \alpha = \gamma^*/\mu_\infty \quad \text{and} \quad T_r = T_\infty - 1/\gamma^*\,. \tag{41}$$

In the above relation (41), both α and T_r are constants and their values depend on the reference state and γ^*, a thermal property of the fluid. For air, for instance,

$$\frac{1}{\mu} = -123.2(T - 742.6) \qquad \text{based on} \qquad T_\infty = 293\,^\circ\text{K}\,(20^\circ\text{C})\,. \tag{42}$$

The data for this correlation were taken from [37]. Although Ling's and Dybb's model is more accurate, its validity is limited to small temperature differences. For instance, Eq. (42) is good to within 1.2% from 278 °K to 373 °K. So, in our study we adopted Sutherland's law for viscosity variation since in high-speed shear layers temperature differences are not small compared with the absolute temperature.

It is known that the best way of removing a small portion of the boundary-layer flow is to develop a continuous porous surface. This solution is not always easy to apply for both structural and aerodynamics difficulties. At the present time, the best methods to approach a continuous suction are to use of spanwise slots or strips of perforated material. Suction has been very often used as an aerodynamic flow control technique to prevent laminar to turbulent boundary-layer transition as well as turbulent flow separation. Application of suction along the leading edge of a wing stabilize the boundary-layer and prevent transition from laminar to turbulent flow over the wing [9]. Small amounts of suction are very efficient for transition control. However, if the suction velocity v_w is too large the boundary-layer could be very thin and the roughness effects be enhanced. As a result, negative effects in terms of drag reduction could be recovered [38]. So, the suction/injection velocity at the wall, v_w, was taken constant and equal to $v_w = \mp 5 \times 10^{-4} u_\infty$ for the case of heating of the wall $(S_w = 2)$, $v_w = \mp 10^{-4} u_\infty$ for an adiabatic wall $(S_w = 1)$ and $v_w = \mp 10^{-4} u_\infty$ for the case of cooling of the wall $(S_w = 0.5)$. This is a valid assumption in order to ensure that the flow with suction or injection at the wall satisfies the simplifying conditions that form the basis of the boundary-layer theory [1]. Also, v_w represents the velocity of suction or injection at the wall according to as $v_w < 0$ or $v_w > 0$, respectively. The case $v_w = 0$ corresponds to an impermeable wall (no suction/injection).

On the other hand, it is known that a large suction volume is uneconomical because a large proportion of the saving in power due to the reduction in drag or to remove the separation point downstream is then used to drive the suction pump. It is, therefore, important to determine the minimum suction volume or the location of suction zone, in the case of localized suction, which is required in order to control the boundary-layer turbulent flow. Interesting information concerning the influence of the suction location on the stability in boundary-layers have been obtained using the nonlinear Parabolized Stability Equations (PSE) approach [16]. The results obtained were related to a flat plate flow with a free stream velocity of 50 m/s. Suction was applied over a streamwise extent of 10 cm with a vertical suction velocity v_w equal to -1 cm/sec. Also, fundamental wind tunnel experiments performed by Reynolds and Saric [15] indicated that suction is more effective when applied at Reynolds numbers close to the lower branch of the neutral curve, in qualitative agreement with previous theoretical results. Finally, measurements carried out on an 8% thick symmetrical aerofoil showed that continuous suction is most effective when it is confined to the upper side of the

wing and when it extends over a region of $0.15\,\ell$ approximately [1]. So, in order to examine the influence of localized suction/injection on the turbulent boundary-layer, in our study we also applied continuous suction/injection in a region confined between $x = a = 0$ and $x = b = 1.2$ m (localized suction). In order to avoid difficulties associated with discontinuities in the region of the boundary surface, simple smoothing functions were introduced for the suction/injection velocity $v_w(x)$ at the wall which can be written as

$$v_w(x) = \frac{1}{2}\, v_0[1 + \tanh\beta(x-a)] \qquad 0 < x \leq \frac{a+b}{2}\,, \tag{43}$$

and

$$v_w(x) = \frac{1}{2}\, v_0[1 - \tanh\beta(x-b)] \qquad x > \frac{a+b}{2}\,, \tag{44}$$

where $a = 0, b = 1.2\,\text{m}, \beta = 10$ and v_0 is a constant suction/injection velocity according to as $v_0 < 0$ or $v_0 > 0$, respectively. This suction/injection velocity v_0 was taken equal to $\mp 5 \times 10^{-4} u_\infty$ in the case of an adiabatic wall ($S_w = 1$), $v_0 = \mp 10^{-3} u_\infty$ for the case of heating of the wall ($S_w = 2$) and $v_0 = \mp 5 \times 10^{-4} u_\infty$ for the case of cooling of the wall ($S_w = 0.5$).

5 Results and discussion

To show the effect of heat and mass transfer on the compressible turbulent boundary-layer flow, with adverse pressure gradient, numerical calculations carried out for different values of the parameters entering into the problem under consideration. The obtained results that are shown on figures concern the velocity field, the temperature field ($S_w \neq 1$), the local skin-friction coefficient C_{fx} and the local Stanton number $\text{St}_x (S_w \neq 1)$. These two last quantities are very important for engineering purposes and can be defined by the following relations:

$$C_{fx} = \frac{\tau_w}{\frac{1}{2}\,\varrho_e u_e{}^2} \qquad \text{and} \qquad \text{St}_x = \frac{\dot{q}_w}{\varrho_e (H_w - H_e)\, u_e}\,, \tag{45}$$

where

$$\tau_w = \left[\mu \frac{\partial u}{\partial y}\right]_{y=0} \qquad \text{and} \qquad \dot{q}_w = -\left[k \frac{\partial T}{\partial y}\right]_{y=0}. \tag{46}$$

Using Eqs. (19), (20), (21) and (25) these quantities can be written as

$$C_{fx} = \frac{2C_w}{\sqrt{\text{R}_x}}\, f_w'' \qquad \text{and} \qquad \text{St}_x = \frac{C_w S_w'}{\text{Pr}\sqrt{\text{R}_x}(1 - S_w)} \quad (S_w \neq 1)\,, \tag{47}$$

where $f_w'' = f''(x, 0)$ is the dimensionless wall-shear parameter, $S_w' = S'(x, 0)$ is the dimensionless wall heat-transfer parameter and $S_w = H_w/H_e$ is the dimensionless total-enthalpy ratio on the wall or heat-transfer parameter. The case $S_w = 1$ corresponds to a flow with no heat transfer between the wall and the fluid (adiabatic flow) and in such a case it is worth examining only the velocity field as well as the local skin-friction coefficient.

(i) Adiabatic wall ($S_w = 1$)

Figures 1 and 2 show the variations of the dimensionless mean velocity profiles $f'(\eta)$, at a typical distance $x = 2.0$ m from the leading edge of the plate, for $M_\infty = M_{\text{inf}} = 0.75$ and 3.0,

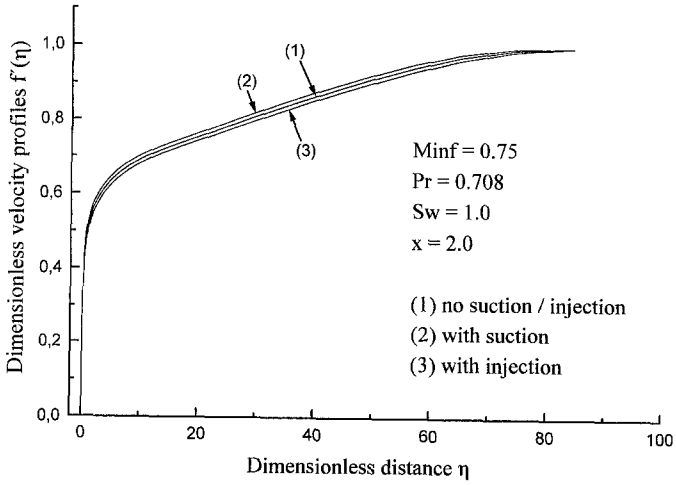

Fig. 1. Variations of dimensionless velocity profiles $f'(\eta)$ for $S_w = 1$

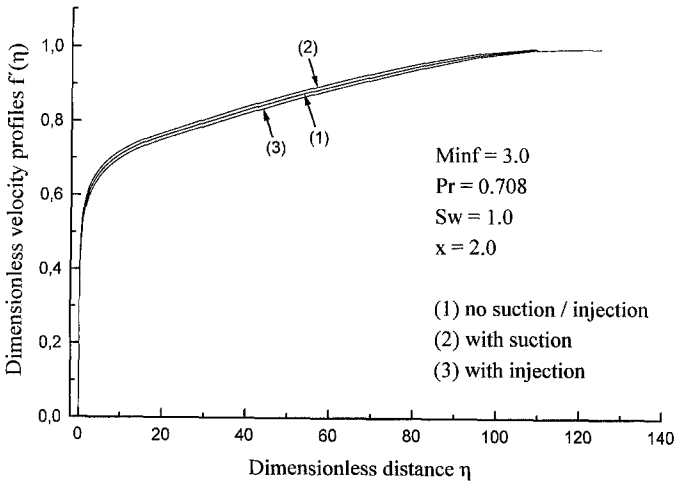

Fig. 2. Variations of dimensionless velocity profiles $f'(\eta)$ for $S_w = 1$

respectively. The curves correspond to the case of no suction/injection (impermeable wall) (1), to the case of suction (2) and to the case of injection (3). The velocity profiles $f'(\eta)$ are affected by the suction/injection velocity applied on the wall as well as by the free-stream Mach number M_∞. It is also observed that the momentum boundary-layer thickness increases significantly with the increase in the free-stream Mach number. The variations of the local skin-fiction coefficient $C_{fx}(C_{fx} \times 10^3)$, with the distance x from the leading edge of the plate, are presented in Figs. 3 to 6 for different values of M_∞ and for the case of continuous or localized suction/injection. The case of an impermeable wall is also presented in these figures. It is concluded from Fig. 3 that application of injection helps in reducing the frictional drag but the separation point moves downstream only in the case of suction and this is more evident for higher values of the free-stream Mach number. Figure 4 shows the variations of the local skin-friction coefficient $C_{fx}(\times 10^3)$ with the distance x along the plate, for different values of the free-stram Mach number M_∞, mainly for the case of an impermeable wall. It is evident that an increase in M_∞ leads to a decrease in the values of C_{fx} and at the same time the separation point moves downwards the limiting surface. To quantify this effect of compressibility on the separation point it is worth mentioning that when M_∞ increases from 0.375 to 0.75 the separation point moves from $x^* = 4.289$ m to $x^* = 4.395$ m. Also, a further

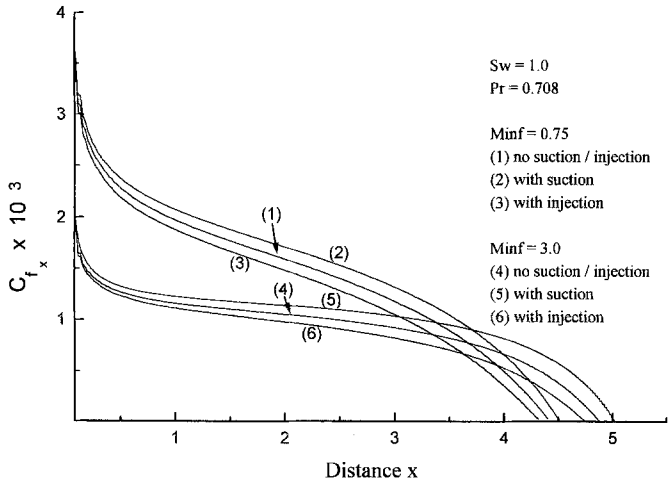

Fig. 3. Variations of local skin-friction coefficient $C_{fx}(\times 10^3)$ for $S_w = 1$

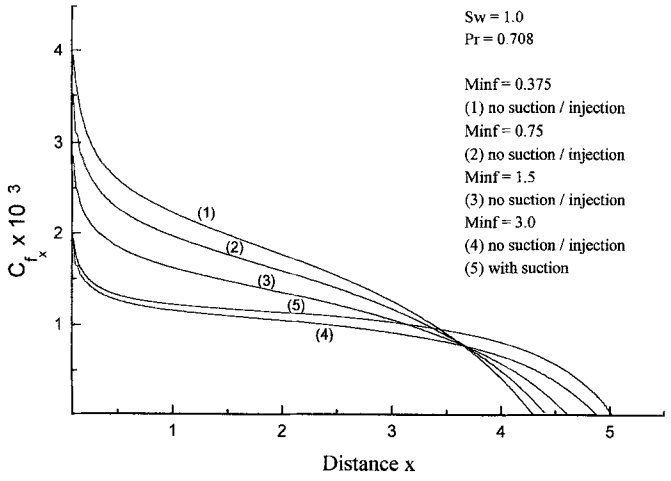

Fig. 4. Variations of local skin-friction coefficient $C_{fx}(\times 10^3)$ for $S_w = 1$

increase of M_∞ from 0.75 to 1.5 and to 3.0 moves the separation point from $x^* = 4.395$ m to $x^* = 4.579$ m and $x^* = 4.868$ m, respectively. On the other hand, when $M_\infty = 3.0$ application of suction helps in removing the separation point from $x^* = 4.868$ m to $x^* = 5.026$ m. Finally, the effect of suction/injection, continuous or localized, on C_{fx} is shown in Fig. 5 for $M_\infty = 2.0$. From this figure it is verified, once more, the effect of suction/injection on the local skin-friction coefficient C_{fx} and the separation point. By blowing air through the permeable wall the skin friction, in case of turbulent boundary-layers, can be reduced and the effect is actually based on thickening the boundary-layer. However, the separation point moves towards the leading edge in the case of injection whereas it moves downwards the plate in the case of suction. What is more interesting though, is the effect of localized suction/injection on C_{fx} and the separation point. By applying localized suction, for instance, from the leading edge up to the point $x = 1.2$ m with a velocity of suction $v_w(x)$ given by the expressions (43) and (44) the separation point moves downwards the plate and at the same time C_{fx} is smaller than the corresponding one in the case of continuous suction, at least for $x > 1.5$ m. This fact could be proved very useful for applications in aerodynamics. It must be emphasized, how-

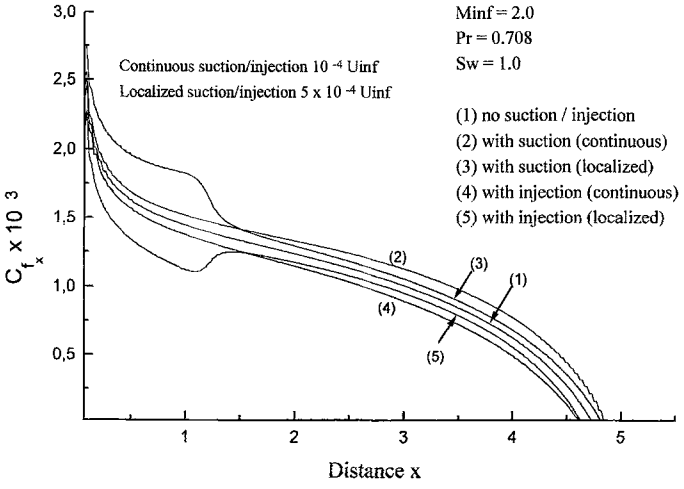

Fig. 5. Variations of local skin-friction coefficient $C_{fx}(\times 10^3)$ for $S_w = 1$

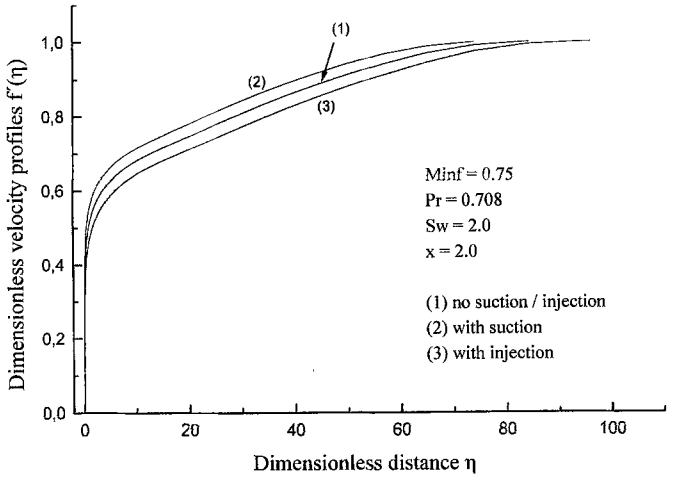

Fig. 6. Variations of dimensionless velocity profiles $f'(\eta)$ for $S_w = 2$

ever, that the suction rate coefficient $C_q = |v_0|/u_\infty$, in the case of localized suction/injection, is five times greater than the corresponding one in the case of continuous suction/injection all over the plate.

(ii) Heating of the wall $(S_w > 1)$

The variations of the dimensionless velocity profiles $f'(\eta)$ with the dimensionless boundary-layer distance η, at a typical distance $x = 2.0$ m from the leading edge, are shown in Figs. 6 and 8 for $M_\infty = 0.75$ and $M_\infty = 3.0$, respectively. The corresponding variations of the dimensionless total-enthalpy ratio S (dimensionless temperature) are shown in Figs. 7 and 9. From these figures it is concluded that the dimensionless viscous or thermal boundary-layer thickness η_e increases as the free-stream Mach number increases. It is worth nothing here though, that the effect of suction/injection in the velocity field is greater in the case of heating of the wall $(S_w = 2.0)$ than that in the case of an adiabatic wall $(S_w = 1)$. The main reason for this difference is the fact that in this case $(S_w = 2.0)$ the suction/injection rate coefficient $C_q = |v_0|/u_\infty$ is five times greater than the corresponding one in the case of an adiabatic wall $(S_w = 1)$. To quantify this effect we refer that in the case of an adiabatic wall $(S_w = 1)$ and when M_∞ is equal to 0.75 (Fig. 1) and the dimensionless boundary-layer distance η is equal,

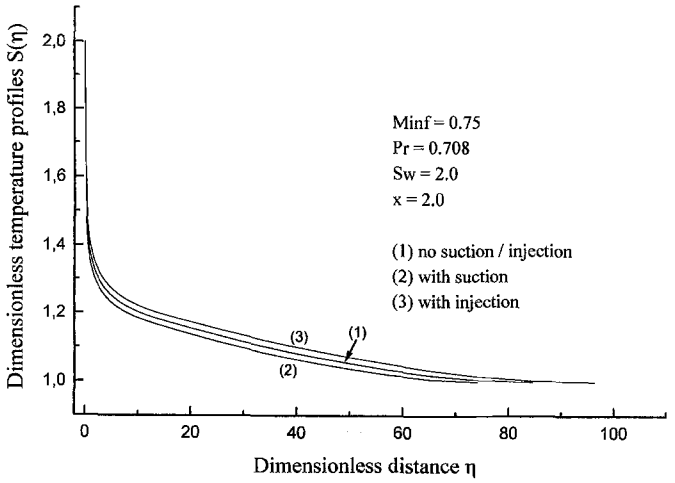

Fig. 7. Variations of dimensionless temperature profiles $S(\eta)$ for $S_w = 2$

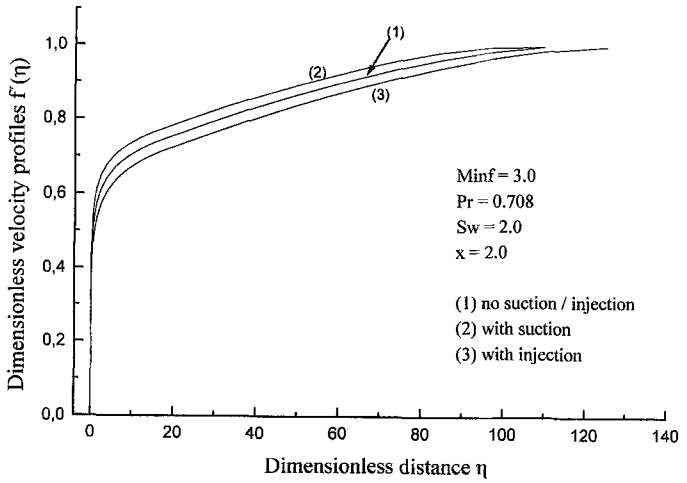

Fig. 8. Variations of dimensionless velocity profiles $f'(\eta)$ for $S_w = 2$

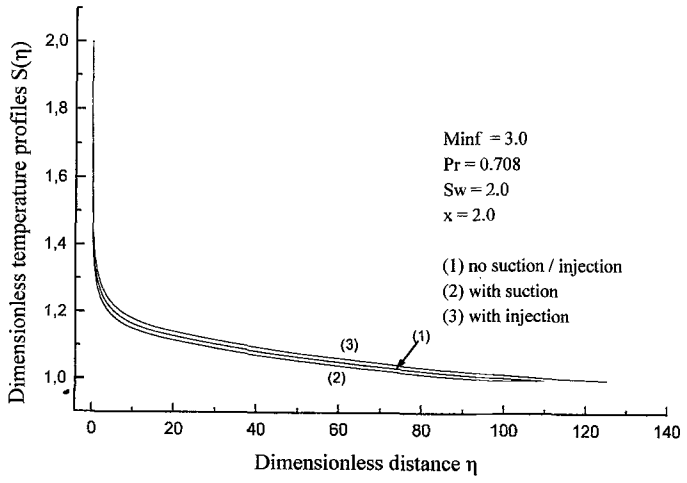

Fig. 9. Variations of dimensionless temperature profiles $S(\eta)$ for $S_w = 2$

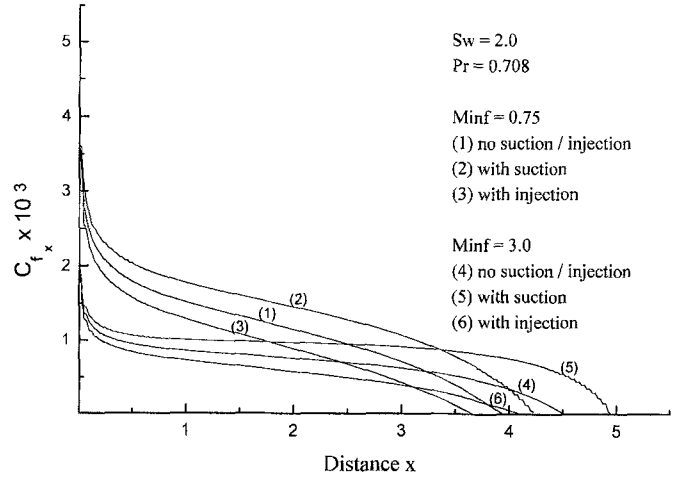

Fig. 10. Variations of local skin-friction coefficient $C_{fx}(\times 10^3)$ for $S_w = 2$

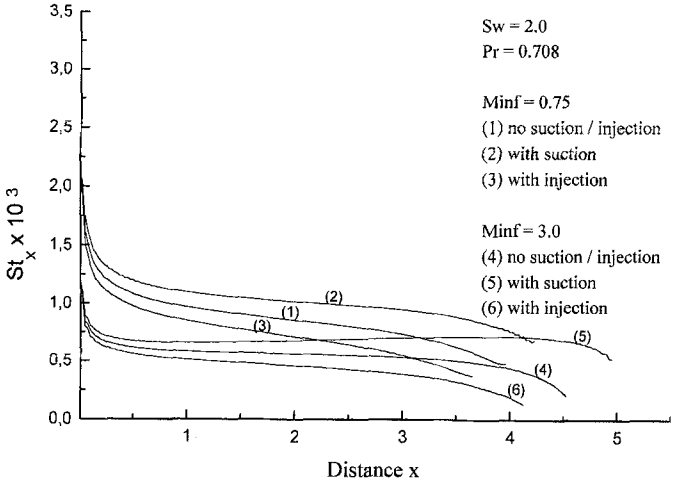

Fig. 11. Variations of local Stanton number $\mathrm{St}_x(\times 10^3)$ for $S_w = 2$

for instance, to 40, application of injection helps in decreasing $f'(\eta)$ by 1.8% with respect to its value in the case of an impermeable wall. The corresponding decrease in the case of heating the wall ($S_w = 2.0$, Fig. 6) is 4%, though. On the other hand, the influence of suction/injection on the dimensionless temperature profiles $S(\eta)$ is almost negligible as the free-stream Mach number increases. Quantitatively, for $\eta = 40, \mathrm{M}_\infty = 0.75$ and $S_w = 2.0$ (Fig. 7), application of suction, for instance, decreases $S(2.0, 40)$ by 1.58%, whereas the corresponding decrease when $\mathrm{M}_\infty = 3.0$ (Fig. 9) is only 1.56%.

Figure 10 shows the variation of the local skin-friction coefficient, with the distance x along the wall, for $\mathrm{M}_\infty = 0.75$ and $\mathrm{M}_\infty = 3.0$ for the case of an impermeable wall as well as for the case of a continuous suction/injection. It is observed that in this case too ($S_w = 2.0$), application of injection helps in reducing C_{fx} but the separation point moves downstream the plate in the case of suction and this is more evident for higher values of M_∞. Quantitatively, for $\mathrm{M}_\infty = 0.75$, the separation point moves from $x^* = 3.96$ m, in the case of an impermeable wall, to $x^* = 4.23$ m in the case of suction, whereas the corresponding values of x^* for $\mathrm{M}_\infty = 3.0$, are $x^* = 4.51$ m and $x^* = 4.95$ m, respectively.

The variation of the heat transfer coefficient, expressed as a local Stanton number, defined by Eq. (47), with the distance x from the leading edge up to separation point, are presented in

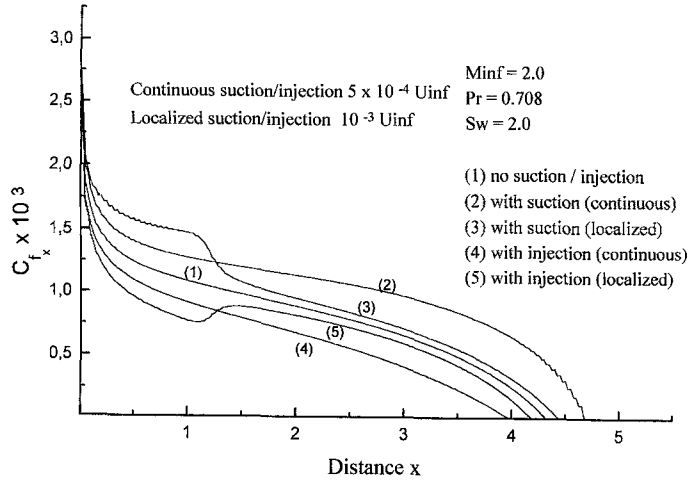

Fig. 12. Variations of local skin-friction coefficient $C_{fx}(\times 10^3)$ for $S_w = 2$

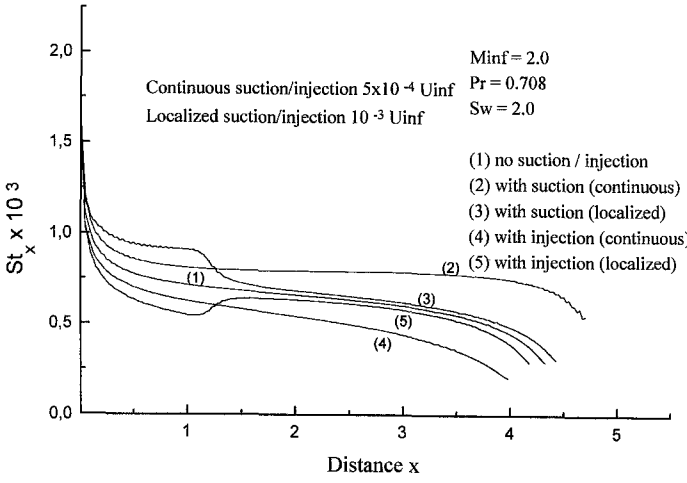

Fig. 13. Variations of local Stanton number $\mathrm{St}_x(\times 10^3)$ for $S_w = 2$

Fig. 11. It is concluded from this figure that St_x is affected by compressibility as well as by the suction/injection velocity imposed at the wall. It is worth emphasizing here however that, when $\mathrm{M}_\infty = 3.0$ and over a large region of the plate, application of suction (curve No 5) helps in increasing the heat transfer coefficient whereas the opposite is true for all the other cases. Finally, Figs. 12 and 13 show the variations of the local skin-friction coefficient and the local Stanton number, respectively, with the distance x along the plate in the case of continuous and localized suction/injection for $\mathrm{M}_\infty = 2.0$. Qualitatively the variation of C_{fx} with x is similar to that in the case of an adiabatic wall ($S_w = 1$, Fig. 5). However, in this case (heating of the wall) at every distance x along the wall, C_{fx} is always less than the corresponding one in the case of an adiabatic wall and consequently the separation point x^* moves towards the leading edge. It must be emphasized also that when the wall is heating ($S_w = 2.0$), the displacement of the separation point, in the case of localized suction or injection, with respect to continuous suction/injection, is greater than the corresponding one in the case of an adiabatic wall ($S_w = 1.0$). On the other hand, the local Stanton number decreases as the distance x

from the leading edge increases for all cases except for the case of continuous suction where St_x is almost constant over a large region over the plate.

(iii) Cooling of the wall ($S_w < 1$)

The variations of the dimensionless velocity and temperature profiles with the dimensionless boundary-layer distance η, at a typical distance $x = 2$ m from the leading edge of the limiting porous surface, are shown in Figs. 14, 16 and in Figs. 15, 17 for $\mathrm{M}_\infty = 0.75$ and 3.0, respectively. The variations of these quantities are similar, qualitatively, to those in the case of heating of the wall ($S_w = 2.0$) and any further discussion seems to be unnecessary. However, it is worth emphasizing that, quantitatively, the influence of the suction/injection on the velocity field and temperature field is greater for $S_w = 2.0$ and less for $S_w = 0.5$. This is a consequence of the fact that the velocity of suction/injection is $v_w = \mp 5 \times 10^{-4} u_\infty$ for the case of heating of the wall ($S_w = 2.0$) whereas $v_w = \mp 10^{-4} u_\infty$ for the case of cooling of the wall ($S_w = 0.5$). To be more specific, in the case of the velocity field for instance, when $\eta = 40, \mathrm{M}_\infty = 0.75$ and $S_w = 2.0$ (Fig. 6) application of injection decreases $f'(2.0, 40)$ by 4.45%, whereas the corresponding decrease when $S_w = 0.5$ (Fig. 14) is only 2.55%.

Figures 18 and 19 show the variations of the local skin-friction coefficient and the local Stanton number, respectively, for $\mathrm{M}_\infty = 0.75$ and $\mathrm{M}_\infty = 3.0$, whereas Figs. 20 and 21 show the variations of the same quantities, for $\mathrm{M}_\infty = 2.0$, in the case of continuous or localized suc-

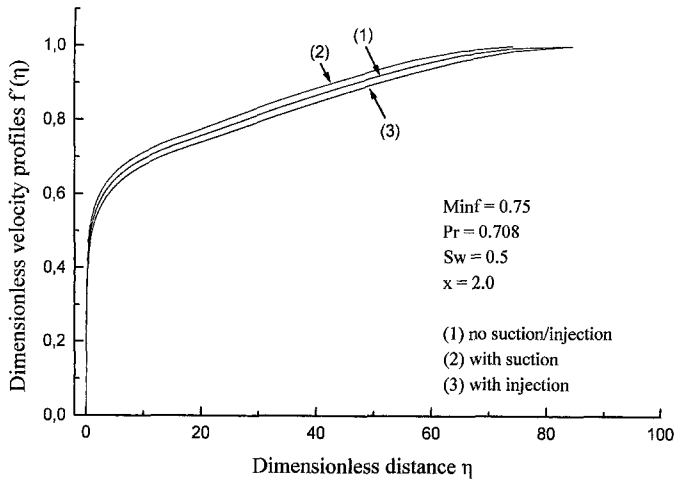

Fig. 14. Variations of dimensionless velocity profiles $f'(\eta)$ for $S_w = 0.5$

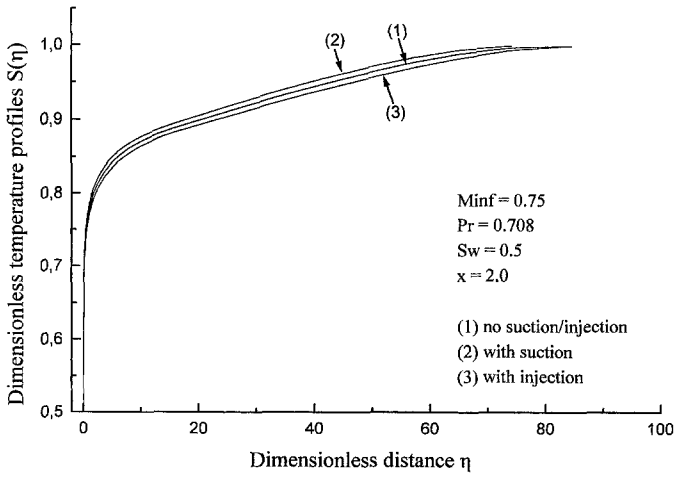

Fig. 15. Variations of dimensionless temperature profiles $S(\eta)$ for $S_w = 0.5$

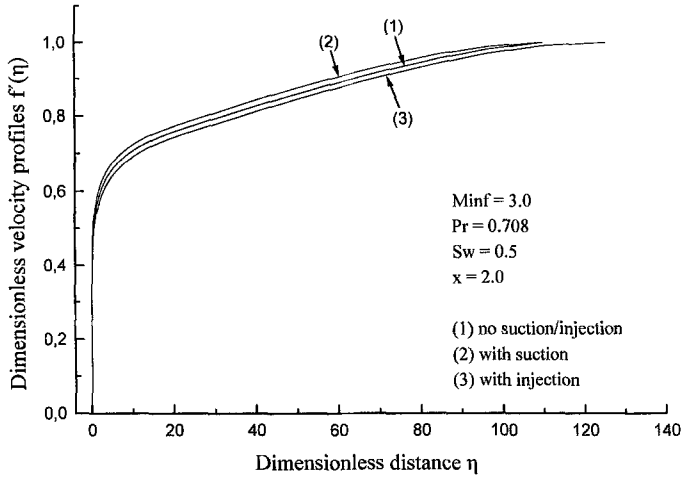

Fig. 16. Variations of dimensionless velocity profiles $f'(\eta)$ for $S_w = 0.5$

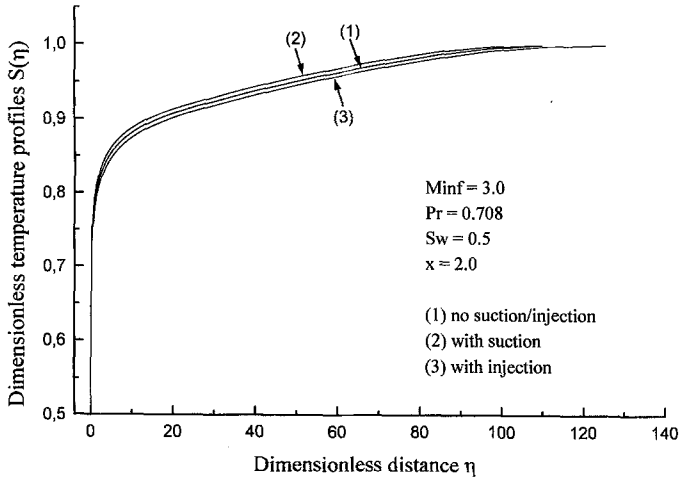

Fig. 17. Variations of dimensionless temperature profiles $S(\eta)$ for $S_w = 0.5$

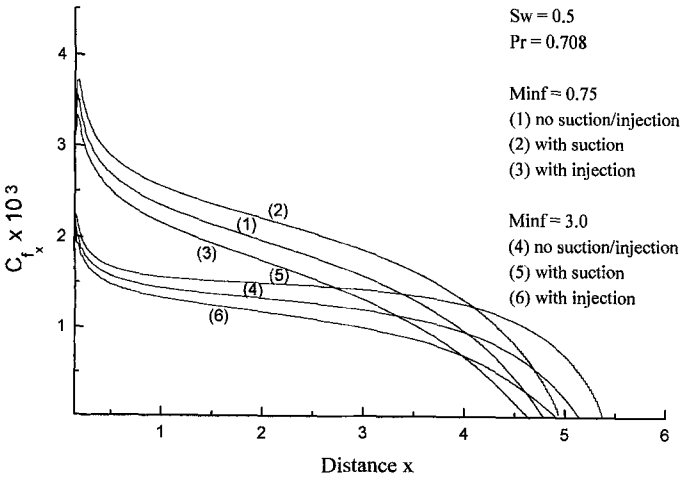

Fig. 18. Variations of local skin-friction coefficient $C_{fx}(\times 10^3)$ for $S_w = 0.5$

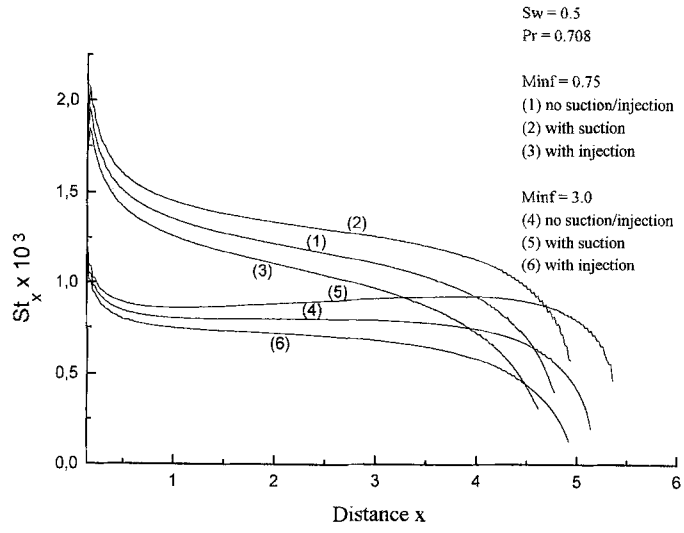

Fig. 19. Variations of local Stanton number $\mathrm{St}_x(\times 10^3)$ for $S_w = 0.5$

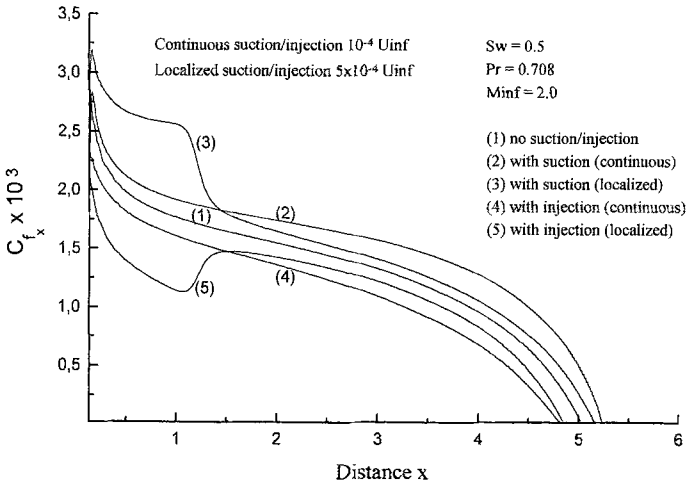

Fig. 20. Variations of local skin-friction coefficient $C_{fx}(\times 10^3)$ for $S_w = 0.5$

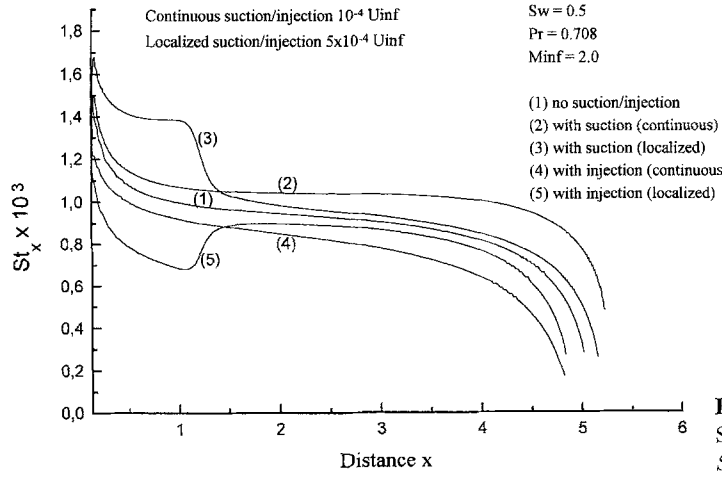

Fig. 21. Variations of local Stanton number $\mathrm{St}_x(\times 10^3)$ for $S_w = 0.5$

tion/injection. The variations of the above mentioned quantities, with the distance x along the limiting porous surface, are similar to those in the case of a heating of the wall ($S_w = 2.0$) presented in Figs. 10–13. However, it is worth mentioning that in the present case ($S_w = 0.5$) the distance x^* of the separation point from the leading edge of the plate, is always greater than the corresponding one in the case of a heating of the wall ($S_w = 2.0$) although the velocity of suction/injection in that case ($S_w = 2.0$) is five times greater than the corresponding one in the present case ($S_w = 0.5$). For instance, when $S_w = 2.0$ and $M_\infty = 3.0, x^* = 4.96$ m in the case of suction (curve (5), Fig. 10) whereas the corresponding value of x^*, in the case of cooling of the wall ($S_w = 0.5$), is $x^* = 5.36$ m (curve (5), Fig. 18). So, it is concluded that the influence of suction/injection on the displacement of the separation point is more effective in the case of cooling of the wall than that in the case of heating of the wall.

6 Concluding remarks

The numerical investigation of the two-dimensional turbulent boundary-layer compressible flow, over a finite smooth and permeable limiting surface, with an adverse pressure gradient and heat and mass transfer showed that:

Adiabatic wall ($S_w = 1$)

(i) The velocity field is significantly affected by the suction/injection velocity applied on the wall as well as by the free-stream Mach number.
(ii) Application of injection helps in reducing the frictional drag but the separation point moves downstream in the case of suction.
(iii) By applying localized suction the separation point moves downwards the wall and the local skin-friction coefficient is smaller than the corresponding one in the case of continuous suction.

Heating of the wall ($S_w = 2.0$)

(i) Due to higher values of the suction/injection velocity, imposed at the wall, in the present case, the effect of suction/injection on the velocity field is more evident than that in the case of an adiabatic wall.
(ii) The effect of suction/injection on the temperature field becomes less evident as the free-stream Mach number increases.
(iii) The local skin-friction coefficient reduces in the case of injection but the distance x^* of the separation point from the leading edge increases in the case of suction and this is more evident for higher values of the free-stream Mach number.
(iv) The local Stanton number is affected by compressibility as well as by the suction/injection velocity imposed at the wall.
(v) Due to different values of the suction/injection velocity, imposed at the wall, the displacement of the separation point, in the case of localized suction/injection, with respect to continuous suction/injection, is greater than the corresponding one in the case of an adiabatic wall.

Cooling of the wall ($S_w = 0.5$)

(i) The variations of the fundamental quantities of the flow field are qualitatively similar to those in the case of heating of the wall ($S_w = 2.0$)

(ii) The influence of the suction/injection on the velocity and temperature field is not so effective as in the case of heating of the wall.
(iii) The influence of suction/injection on the displacement of the separation point is more effective than the corresponding one in the case of heating of the wall.

Acknowledgement

This work was partially supported by the AGARD support project G96, Contract No. 458G96A.

References

[1] Schlichting, H.: Boundary-layer theory, trans. by Kestin J. 7th ed. New York: McGraw-Hill, 1979, p. 635.
[2] Gad-el-Hak, M., Bushnell, D. M.: Separation control: review. J. Fluid Eng., Transactions of the ASME **113,** 5–29 (1991).
[3] Bushnell, D. M.: Longitudinal vortex control-techniques and applications. The 32nd Lanchester Lecture, Aeronautical Quartely, pp. 293–312, October 1992.
[4] Gad-el-Hak, M., Bushnell, D. M.: Status and outlook of flow separation control, AIAA Paper 91-0037 (1991).
[5] Kline, S. J., Robinson, S. K.: Turbulent boundary-layer structure: progress, status and challenges, in: Structure of Turbulence and Drag Reduction (Gyr, A., ed.). IUTAM Symposium Zürich, Springer, pp. 3–22, 1990.
[6] Robinson, S. K.: Coherent motions in the turbulent boundary layer. Ann. Rev. Fluid Mech. **23,** 603–639 (1991).
[7] Blackwelder, R. F.: The eddy structures in bounded shear flows. In: Special course on skin friction drag reduction (Cousteix, J., ed.). AGARD Report 786, Paper 6, 1992.
[8] Kim, J. J.: Study of turbulence structure through numerical simulations: the perspective of drag and reduction. In: Special course on skin friction drag reduction (Cousteix, J., ed.). AGARD Report 786, Paper 7, 1992.
[9] Arnal, D.: Control of laminar-turbulent transition for skin friction drag reduction. In: Control of flow instabilities and unsteady flows (Meier, G. and Schnerr, G., eds.) pp. 119–153, CISM Courses and Lectures No. 369, Udine, 1995. Springer: Wien New York, 1996.
[10] Gad-el-Hak, M.: Flow control by suction. In: Structure of turbulence and drag reduction (Gyr, A., ed.) IUTAM Symposium Zürich, Switzerland, Springer, pp. 357–360, 1990.
[11] Sokolov, M., Antonia, R. A.: Response of a turbulent boundary layer to intensive suction through a porous strip. In: Proc. 9th symposium on turbulent shear flows. Kyoto Japan, Paper 5–3, 1993.
[12] Wilkinson, S. P., Anders, J. B., Lazos, B. S., Bushnell, D. M.: Turbulent drag reduction research of NASA Langlay: progress and plans. Int. J. Heat Fluid Flow **9,** 266–277 (1988).
[13] Gad-el-Hak, M., Blackwelder, R. F.: Selective suction of controlling bursting events in a boundary layer. AIAA Journal **27** (3), 308–314 (1989).
[14] Myose, R. Y., Blackwelder, R. F.: Control of streamwise vortices using selective suction, AIAA Journal **33** (6), 1076–1080 (1995).
[15] Reynolds, W. S., Saric, W. S.: Experiments on the stability of the flat plate boundary layer with suction, AIAA Paper 82–1026, 1982.
[16] Casalis, G., Copie, M. L., Airiau, Ch., Arnal, D.: Nonlinear analysis with PSE approach. In: IUTAM Symposium on nonlinear instability and transition in three-dimensional boundary layers. (Duck, P. W. and Hall, P., eds.), pp. 217–254. IUTAM Symposium, Manchester, UK, 17–20 July 1995. Kluwer Academic Publishers: Dordrecht, 1996.
[17] Hefner, J. N., Bushnell, D. M.: Surface drag reduction via surface mass injection. In: Viscous drag reduction in boundary layers. Progress in Astronautics and Aeronautics **123,** AIAA Washington, D. C., pp. 457–476, 1990.

[18] Cummings, R. M., Schiff, L. B., Duino, J. D.: Experimental investigation of tangential slot blowing on a generic chined forebody. Journal of Aircraft **32** (4), 812–824 (1995).
[19] Sumitani, Y., Kasagi, N.: Direct numerical simulation of turbulent transport with uniform wall injection and suction. AIAA Journal **33** (7), 1220–1228 (1995).
[20] Spalart, P. R., Moser, R. D., Rogers, M. M.: Spectral methods for the Navier-Stokes equations with one infinite and two periodic directions. J. Comp. Phys. **96,** 297–324 (1991).
[21] Spalart, P. R., Watmuff, J. H.: Experimental and numerical investigation of a turbulent boundary layer with pressure gradients. J. Fluid Mech. **249,** 337–371 (1993).
[22] Marusic, I., Perry, A. E.: A wall-wake model for the turbulence structure of boundary layers, Part 2. Further experimental support. J. Fluid Mech. **298,** 389–407 (1995).
[23] Spalart, P. R., Coleman, G. N.: Numerical study of a separation bubble with heat transfer. Europ. J. Mech. **B 16,** 169–189 (1997).
[24] Cebeci, T., Bradshaw, P.: Physical and computational aspects of convective heat transfer. 1st ed. New York: Springer, 1984, p. 52.
[25] Cebeci, T., Smith, A. M. O.: Analysis of turbulent boundary layers. New York: Academic Press, 1974.
[26] Minkowycz, W. J., Sparrow, E. M., Schneider, G. E., Pletcher, R. H.: Handbook of numerical heat transfer. 1st ed. New York: Wiley, 1988, p. 120.
[27] Cebeci, T.: A model for eddy conductivity and turbulent Prandtl number. ASME Journal of Heat Transfer **95,** 227–234 (1973).
[28] Chen, C. J., Chiou, J. S.: Laminar and turbulent heat transfer in the pipe entrance region for liquid metals. Int. J. Heat Mass Transfer **24,** 1179–1189 (1981).
[29] Jischa, M., Rieke, H. B.: About the prediction of turbulent Prandtl and Schmidt number. Int. J. Heat Mass Transfer **22,** 1547–1555 (1979).
[30] Kays, W. M., Crawford, M. E.: Convective Heat and Mass Transfer. 3rd edn. New York: McGraw-Hill, 1993.
[31] Weigand, B., Ferguson, J. R., Crawford, M. E.: An extended Kays and Crawford turbulent Prandtl number model. Int. J. Heat Mass Transfer **40,** (17) 4191–4196 (1997).
[32] Schreier, S.: Compressible flow. New York: Wiley 1982.
[33] Keller, H. B.: A new difference scheme for parabolic problems. Numerical solutions of partial differential equations, II. (Bramble, J., ed.): New York: Academic Press, 1970.
[34] Rees, D. A. S.: Three-dimensional free convection boundary layers in porous media induced by a heated surface with spanwise temperature variations. Transactions ASME, J. Heat Transfer **119,** 792–798 (1997).
[35] Rees, D. A. S.: Free convective boundary-layer flow from a heated surface in a layered porous medium. Journal of Porius Media (to appear) (1999).
[36] Ling, J. X., Dybbs, A.: Forced convection over a flat plate submersed in a porous medium: variable viscosity case, Paper 87-WA/HT-23, New York, ASME 1987.
[37] CRC Handbook of Chemistry and Physics (67th ed.), CRS Press, Boca Raton, FL, 1986–1987.
[38] Meier, G. E. A., Schnerr, G. H.: Control of flow instabilities and unsteady flows. CISM Courses and Lectures, No. 369, 1996.

Authors' address: N. G. Kafoussias and M. A. Xenos, Department of Mathematics, Section of Applied Analysis, University of Patras, 26500 Patras, Greece